# Iridium oxide redox gradient material: O*perando* XRay absorption of Ir gradient oxidation states during $IrO_x$ bipolar electrochemistry

Laura Fuentes-Rodriguez[1,2], Llibertat Abad[2], Laura Simonelli[3], Dino Tonti[1], Nieves Casañ-Pastor*[1]

[1] Institut de Ciencia de Materials de Barcelona, CSIC, Campus UAB, 08193 Bellaterra, Barcelona, Spain

[2] Centre Nacional de Microelectrónica, Institut de Microelectrónica de Barcelona-CSIC, Campus UAB, 08193 Bellaterra, Barcelona, Spain

[3] ALBA Synchrotron Light Facility, Carrer de la Llum 2-26, 08290 Cerdanyola del Vallès, Spain

Corresponding author: nieves@icmab.es

**Abstract**

Electrodeposited iridium oxide ($K_{1.7}IrO_{0.8}$ $(OH)_{2.2} \cdot 1.8$ $H_2O$; also called $IrO_x$) is among the best substrates for neural growth, decreasing impedance and stimulating cell growth, when used as connected electrode. Without direct contact, it has been proven to stimulate neurons, through a bipolar mechanism related to the conducting character of the material in presence of remote electric fields. The remote wireless electrostimulation that arises from it is of large significance in clinical applications. Ionic intercalation simultaneous to iridium oxidation state changes at the induced $IrO_x$ cathode, and the formation of a redox and ionic gradient at the $IrO_x$ substrate is envisaged as the most probable explanation for the observed effects on neural cell growth. This work shows the iridium state gradient through XRay absorption spectroscopy (XAS), with significant electrochemical features, and relaxation times, that allow a persistent effect in the material even after the electric field creating the induced dipole is shut down. It also shows a correlated intercalated sodium gradients observed by semiquantitative Energy dispersive XRay analysis (EDX) data. The bipolar effect is proven and yields new evidence for the behavior of other biocompatible neural growth substrates.

**Key words:** Gradient materials, electroactive, bipolar electrochemistry, XRay absorption, Iridium oxide.

## 1. Introduction

Bipolar electrochemistry processes are relatively unusual, although a significant number of features derived from it have been established. Asymmetric electrochromism, nanostructuring specific materials, molecular motors, and more recently directioning neural growth when used as substrate for neurons have been shown [1-12]. Bipolar electrochemistry is based on the induction of dipoles on a conducting material, when it

is immersed in an electrolyte in presence of an external electric field. The borders where electronic conductivity disappears, in contact with the electrolyte, become then the induced anode and cathode of a dipole that opposes the external field. If the induced potential among them is sufficiently large, electrochemical reactions may occur in each of them. $H_2$ and $O_2$ formation from water splitting may be formed at the induced cathode and anode. In addition, electrodeposition of metals at the cathode, or of oxides and other materials at the induced anode are possible. In case of intercalation materials, cation intercalation is possible in the bulk material cathode-side, and deintercalation of cations at the induced anode. A similar anion process becomes possible or combined reactions where solution species react in one side, and the material intercalation occurs at the other side.

Redox gradient materials, on the other hand, are almost unknown, but are particularly relevant when redox intercalation exists in electroactive materials. The electronic gradient that results during polarization of immersed conducting particles and macroscopic pieces offer additional possibilities in materials synthesis [14], nanomotors [9], and allows additional charge transfer mechanisms in electrochemical cells or in energy storage processes (unpublished results). It also creates a directional chemical gradient that has been shown to modify neural cell growth [11].

In particular, anodically deposited iridium oxide may yield to one of such redox gradient cases, with a particularly significant role in bioelectrodes. With direct electrical contact, iridium oxides are optimal electrodes for water splitting and $O_2$ evolution [15], reduction electrocatalysis, additives to carbon felt electrodes [16], or electrochromic and solar cells [17]. It is also the best substrate for neural cell growth in the case of mammalian cell cultures [11, 18]. As a coating of Pt or steel bioelectrodes, it has been shown that anodically deposited iridium oxide, $IrO_x$, decreases inflammation and increases the charge capacity that may be delivered in electrostimulation processes, lowering also the impedance of the bioelectrodes, and the formation of oxygen radicals that are detrimental for cell survival and growth [18-20]. Such charge capacity enhancement is one order of magnitude larger when the oxide is combined with graphitic carbons or nanocarbons [21-24]. The mechanisms acting on cells are not yet understood, but for biocompatible intercalation materials like $IrO_x$, or conducting polymers, it is easily assumed that redox ionic intercalation acts as a safe alternative to radical formation [11, 18].

What is named usually as Iridium oxide, in fact, is several distinct materials, which are obtained by different methods. Crystallized $IrO_2$, obtained by sputtering, anodization of the metal and thermal methods [25], has a dense rutile structure and is less active in terms of electrochemical intercalation processes, given the great compactness of the structure, and mixed valence structures have not been reported for that case. However, electrodeposited $IrO_x$, is a hydrated oxohydroxide of iridium, $(K_{1.7}IrO_{0.8}(OH)_{2.2} \cdot 1.8\ H_2O$, is amorphous and has a density one sixth of the crystalline one [18,26], is a mixed valence material with intercalated $M^+$ ions, and evolves rapidly in presence of an electron beam in Transmission electron microscopy (TEM). The coating has been reported to be a flocculation of $IrO_x$ nanoparticles 2 nm in size [27] based on TEM experiments. However,

now it is known that those 2 nm nanoparticles are really Iridium metal nanoparticles that are formed under the electron beam microscope, especially in the high voltage ones. Low voltage TEM experiments have shown the evolution of the material, from an oxo-hydroxo iridium material containing intercalated potassium, clustering in particles 10 to 20 nm in size, to a hollandite type phase, $K_xIrO_2$ and finally to metallic iridium particles 2 nm in size [28]. Additional data, apart from TEM, shows that the deposited material is amorphous and forms in presence of ions like $K^+$ (or $Na^+$) yielding the reproducible formula $K_{1.7}IrO_{0.8}(OH)_{2.2} \cdot 1.8\ H_2O$ [18], mentioned above. It has been proven to exchange $K^+$ and show easy intercalation chemistry with $H^+$, $Na^+$ and $K^+$ [18], and probably $OH^-$, and can be viewed as a hydrated sponge like structure. The anodically resulting dark blue $IrO_x$ coating may still be reduced further with additional $M^+$ intercalation, until a colorless coating is obtained, with a fast electrochromic effect [17] related presumably to the formation of a stoichiometric Iridium (III) oxide.

The blue $IrO_x$ coating is the one that activates neural growth when used as a connected electrode, while undergoing redox chemical changes itself [18, 20, 28]. Without direct electrical contact, when $IrO_x$ is immersed in an electrolyte, as other conducting materials, undergoes the formation of a dipole at their borders in the direction of the external applied field, which in turn induces bipolar electrochemistry effects at the induced anode and cathode of the material [11]. Thus, wireless neural electrostimulation becomes possible[11]. It has been hypothesized that in these cases of intercalation materials, ionic mobility in bipolar electrochemistry conditions may allow the formation of induced ionic gradients within the specific phase, yielding a gradient material, and modifying the cues that drive neural growth. However, each material tested influences differently the growth of neurons, even with similar expected intercalation of ions and gradients. Poly(3,4-ethylenedioxythiophene) polystyrene sulfonate (PEDOT-PSS) favors cathodal turning of dendrites during growth, while $IrO_x$ favors an increase in speed of the dendrite growth when cells grow on a bipolar PEDOT or $IrO_x$, and moderate external driving field [11]. Pure conducting metals like Au have a different growth effect, suggesting that it is not the conducting character the only factor influencing cell growth, neither the effects of the induced dipoles on the surrounding electrolyte. The evaluation of each of the cases is significant to elucidate the role of the material and its chemistry on cell behavior.

Elucidating the changes that occur within the material and the nearby environment would help to pin the factors that influence neural cell behavior. As bipolar electrochemistry effects have been detected [11], the study and characterization of the true existing gradient created for each material used as substrate for neural cell growth is the first focus. In the $IrO_x$ case in particular, gradients in iridium oxidation state, as well as gradients of the corresponding $M^+$ cations intercalated in the material may yield significant evidence of the chemical reactivity changes along the sample, and therefore of the chemical map that cells note when growing on the bipolar material. In particular, for $IrO_x$ it is known that $K^+$, present in the deposited oxohydroxide, is released by simple immersion in water solutions, possibly by exchange with $H^+$. It is also known that in

sodium containing electrolytes, $Na^+$ intercalates upon reduction in $IrO_x$ electrodes [18]. Therefore, in gradient materials, an Energy dispersive XRay Analysis (EDX) study of the spatial gradient of $Na^+$ content along the sample seems adequate to evaluate the ionic gradients that may influence cells growth. Only, electron beam effects must be considered and no high voltage electron beams used. However, precisely because of that risk, XRay absorption studies with spatial resolution are a rather significant alternative to study the ionic gradients. Specifically, Iridium XRay absorption lines are attractive because they may show variations in oxidation state directly in Iridium, along the sample. Previous XPS results on the other hand have shown no sensitivity to changes in Iridium oxidation state [18], neither have spatial resolution, nor the cell fulfils the vacuum requirements for local exploration of the $IrO_x$ surface, so that XPS experiments have not been considered. XRay absorption spectroscopy (XAS) experiments had been carried out before in homogeneous electrodeposited oxo-hydroxo $IrO_x$ coating samples with success [18, 29, 30], evidencing the sensitivity of the absorption energy to various oxidation states including large oxidation phases. In particular, for the potential window that aqueous systems allow, differences have been observed between electrodeposited $IrO_x$ and $IrO_2$ and iridium chlorides [18].

The work reported here shows, both, the space gradient observed in Iridium LIII absorption energies during a bipolar electrochemistry experiment, and the gradients in $Na^+$ local concentrations by EDX in ex-situ conditions. A correlation between both sets of data is made, and also with the parallel optical changes during the bipolar process. *Operando* XAS detection experiments should, allow a real time study of the gradients induced in Iridium oxidation state in bipolar conditions, a study of the time scale of the process, and possibly the relaxation of the gradient as the external electrochemical field is shut down. Thus, this work evidences the existence of a dipole between borders of $IrO_x$ when set unconnected between parallel electrodes in a neutral phosphate buffer electrolyte. The various arrangements and measurement protocols allow to identify the effects of proximity to the driving Pt electrodes. The results show clear evidence of the expected gradient in a range of imposed external potentials. At higher potentials the effect of $H_2$ and $O_2$ evolution at the cathode and anode driving electrodes, of opposed sign than the bipolar effect, is also observed, and is clearly differentiated. Thus, there is a range where an $IrO_x$ gradient material is formed, diffusion along the sample is also seen reaching a significantly stable configuration, and then slowly reoxidizes to a near original material in terms of Iridium oxidation state but containing intercalated $Na^+$. Time evolution yields a time scale in the order of days, explaining the sustained effect in neural cell growth after a short electric field exposition.

## 2. Experimental

12 nm thick Pt coatings on 26 x 74 mm pieces of cyclo-olefin polymers (COP, 188 μm thick Zeonor sheets ZF14–188, Zeonex GmbH) [31] were obtained by thermal evaporation using $Ar^+$ plasma using Pt 99.95% Goodfellow, at 0.6 nm/hour growth, and with control of thickness through a quartz microbalance setting. Pt was deposited on Ø100 mm COP wafer-type piece and on pieces with 2 mm wide vertical stripes (centered 1, 2 or 3

parallel stripes as shown in Figure 1) parallel to the cell main axis dimension, using a vinyl shadow mask. (See Figure 1). Vinyl shadow masks were cut with a Roland GX24-CAMM-1 cutter-plotter (Arista SL, Spain). A wider Pt deposit is made at the upper part of the stripes (26 x 6 mm) to facilitate contact for $IrO_x$ electrodeposition.

Electrodeposition of $IrO_x$ coatings was performed on flat Pt-COP 10 x 30 mm size or on pieces with Pt strips using a dynamic potential sweep method described previously [10] using a solution 0.002 M $IrCl_3$ (99 % Sigma Aldrich), 0.001 M $H_2C_2O_4$ (oxalic acid) and 0.005 M $K_2CO_3$, (98 % and 99% respectively Sigma Aldrich) added in that order. The solution was aged at 37°C during 4 days to allow hydrolysis of iridium ions from the chloride (green) to the oxo species (dark blue), and kept at 4°C until use to prevent further hydrolysis. Deposition was performed by a dynamic applied potential with 50 cycles between 0 and 0.7 V vs Ag/AgCl reference electrode, according to reference [18]. Several flat electrochemical cells set-ups have been built, both for easy visual inspection of color changes in $IrO_x$ materials, and for preparation of gradient $IrO_x$ with intercalated $Na^+$ for EDX. In both cases, 1 $cm^2$ squares of $IrO_x$ electrodeposited on Pt coated COP were immersed in the center of the space between the two parallel flat Pt counterelectrodes 30 mm apart and immersed 6 mm deep, (24 mm wide). The electrolyte was a 0.1 M total phosphate buffer with pH 7.4, prepared from $Na_2HPO_4$ and $NaH_2PO_4$ (both 99% from Sigma Aldrich).

Several rectangular prism electrochemical cells were built for *operando* X-Ray absorption spectroscopy studies at CLAESS beamline at ALBA synchrotron [32]. A wiggler source was monochromatized using a Si (311) double crystal monochromator, while Rh-coated mirrors were used to reject higher harmonics. The beam was focused down to 0.2 x 0.1 $mm^2$ to map the Ir oxidation state gradient. The spectra were acquired along the $IrO_x$ electrodeposited striped at different sample positions in the perpendicular stripe direction. Measurements were done in continuous mode, in a time scale of half a minute by means of a multichannel silicon drift fluorescence detector mounted at 90° respect the incident beam.

Figure 1 depicts the rectangular prism electrochemical cells which have been exploited in the here reported investigation, all of them containing two narrow Pt driving electrodes. The cells were done with four pieces of glass (the narrow lateral sides coated with Ti (5 nm) and Pt (12 nm), and one piece that was made directly by the sample, an $IrO_x$ coating on Pt-COP foil. Such prisms have been inserted on a vacuum-air interface sample holder with kapton windows at 45° respect both the incident beam and the fluorescence detector. It is only through this COP-Pt (12 nm)-$IrO_x$ (170 nm) foil plus the 75 µm kapton windows that the XRay radiation was travelling before detection.

1, 2 and 3 stripe setting, all formed by 2 mm wide vertical stripes, are prepared to detect possible differences between stripes and their positions in the electrochemical cell.

Driving electrodes used in bipolar cells for XAS experiments are Pt (12 nm coating) on Ti (5 nm) on glass microscope slides (prepared in 26 x 74 mm Thermoscientific ™ glass and

cut before use to 5 x 74 mm size), were obtained also by thermal evaporation. Those driving electrodes are set as the narrow sides of the rectangular prism electrochemical cell, that also had the $IrO_x$-Pt-COP piece, a plain glass piece (26 x 74 mm) parallel to it and a bottom glass piece (cut to 6 x 26 mm size). The complete cells are set by gluing the five components (4 sides and bottom) using Silicone CEYS TOTAL Tech R. (Figure 1). The electrolyte, filling 80% of the volume, is the same sodium phosphate buffer described above, and also used for EDX and optical experiments. Possible electrolyte leakage was tested in all cells during 12 hours. Since $IrO_x$ is known to release $K^+$ during immersion, this means that the samples studied did not contain $K^+$ [18].

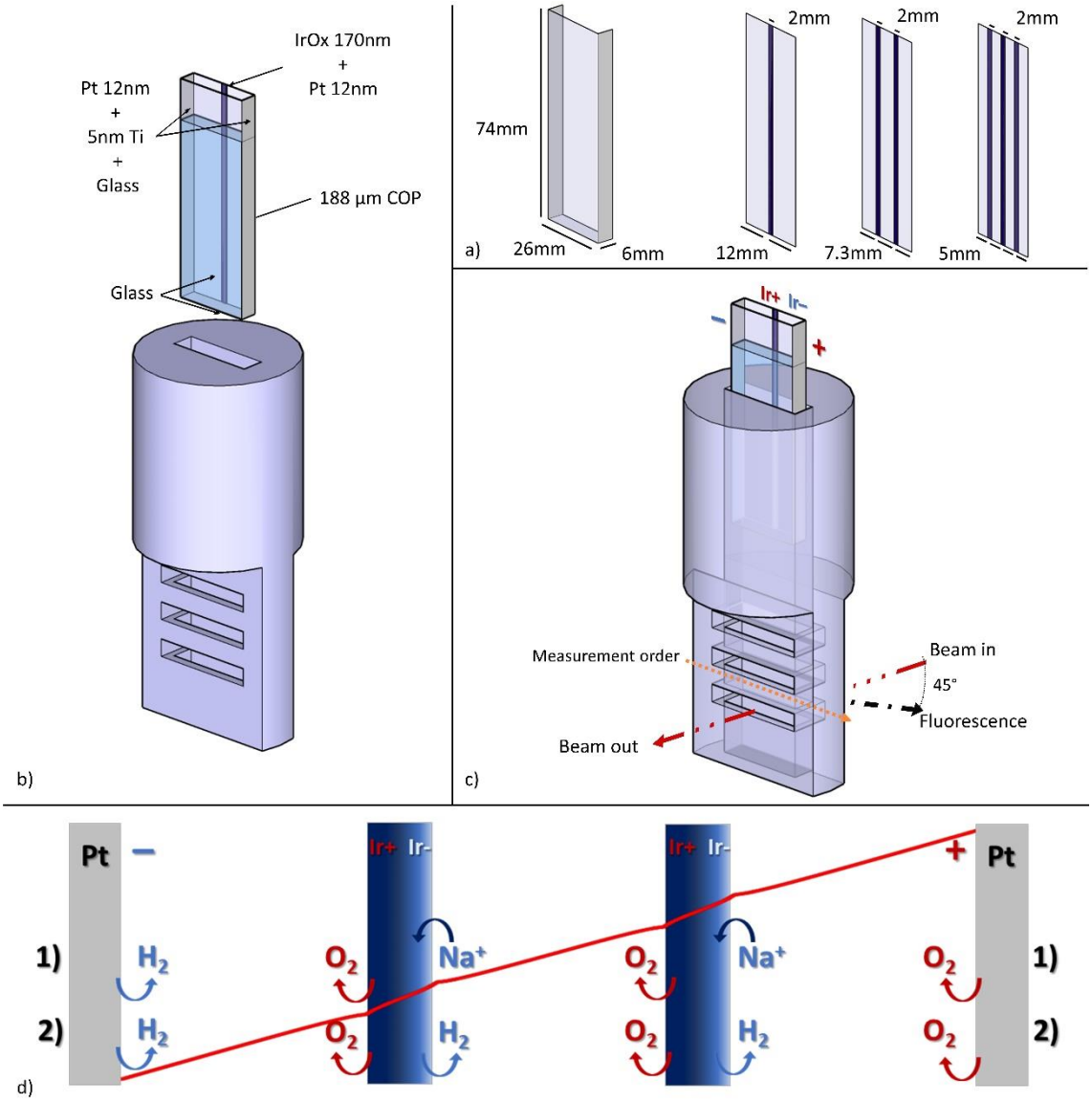


**Figure 1**. a) COP and Glass pieces forming the electrochemical cell set. b) Electrochemical cell inserted in chamber holder (inverted vacuum, the holder will have vacuum in the outer side). The cell is built with a COP piece printed with Pt and $IrO_x$ in 1, 2 or 3 vertical stripes, after cutting the direct electrical contact used for $IrO_x$ deposition, two lateral Pt on Ti-glass electrodes, a front and bottom glass walls. c) Incident beam is adjusted to fit through any of the 3 slits in the holder, and the chamber moves with respect to the beam as indicated by the orange arrow. Slits are sealed by a Mylar film. Detection in fluorescence mode is done at 45° from incident beam to

prevent absorption effect from the aqueous and glass parts of the cell. d) Scheme showing the possible reactions occurring in a two stripe set up, both at the $IrO_x$ coatings and at the driving Pt electrodes, and the voltage profile (red) , 1) at low potentials and 2) at high potentials. Note that there could be a regime in which 1) and 2) may overlap. The profile accounts for a simplified case of constant conductivity $IrO_x$. The reduced part (Ir-) where $Na^+$ intercalates is also getting less conductive, which modifies the zero charge front in the $IrO_x$. At higher potentials also $H_2$ is formed in that induced pole [11].

Connection of the two Pt driving electrodes to an external Biologic VSP potentiostat was made using a U-Shape Pt bulk piece held by steel alligators. Electrical wiring was connected to a feedthrough on a KF40 flange put on top of the inverse vacuum chamber. He flow was inserted in the upper part of the chamber to prevent accumulation of electrolysis gases. Synchronization of electric field application and XAS spatial scans was performed manually. VSP was run using EC-lab software.

References used for beam absorption were a metallic Pt piece, absorbing very near metallic Ir, and commercial $IrO_2$ rutile (99.9% Sigma-Aldrich).

Fluorescence spectra have been collected scanning horizontally, in 3 to 7 positions, in every slit shown in the sample holder (Figure 1) in 45° angle with respect to the incoming photon beam. Absorption intensity profiles were run initially transversal to each stripe showing the smooth mountain shape of all $IrO_x$ coatings. For that reason, the spatial scan for each measurement was adjusted to be slightly inferior to the 2 mm width of the stripe. The positioning stage was adjusted to reproduce the measurement positions in each scan. Thus, each scan measures 3 to 7 spatial positions in every stripe. The direction of the measurement goes from the Pt driving cathode (-) side, which corresponds to $IrO_x$ induced anode (+) towards the $IrO_x$ induced cathode (-) looking towards the driving Pt anode (+). Measurements in several stripes and slits are performed occasionally to evaluate equilibration within the $IrO_x$ sample. In addition, in one case polarity is inverted to check reversibility. For these maps, a beam with an energy slightly above the Iridium LIII line was used. In such energy range, the beamline is stable below 0.1 eV, i.e. energy shifts of around 0.05 eV can be still appreciated when the spectral signal permit, involving an adequate resolution for the energy differences expected in the 1 eV range.

Beam damage on the cell or on the $IrO_x$ coating was evaluated through more than 3 hours beam incidence in the same $IrO_x$ position in absence and presence of electric field. Limits of 2 hours are found for detachment of the $Pt/IrO_x$ coating, when beam incides continuously in the same point, but only on the pole that is positive if field is acting. Possible flaws of electrical connections and the measurement sequence were also checked originally in several scan tests.

Key experiments were run by scanning the sample stripe with the beam (1, 2 and 3 stripes of $IrO_x$ on Pt/COP), with each case mounted in an independent electrochemical cell. 1) First, during a voltage scan (0 to 5 V vs pseudoreference/counterelectrode in the two electrode system), at 4.16 mV/s (a total of 20 min), and relaxation during 5.5 hours. Immediately after, an inversed scan 0 to -5 V was performed with the corresponding

relaxation time. 2) In second place, based on previous results, pulses were considered a better option and consecutive pulses at several voltages during a constant 1 min time were run, followed by 1 hour relaxation time at each voltage, up to 5 V, and after 10 day relaxation, from 7 to 30 V without relaxation. 3) Finally, pulses at the same voltage (5 V) with various pulsing times were performed, followed by 30 min relaxation.

For each resulting spectrum, the raw data has been normalized by subtracting and separating pre-edge and post-edge backgrounds as linear contributions. Fitting to a Gaussian curve with a sigmoidal added function is later performed to reach the energy maximum and FWMH (full width at medium height) for each measurement. Least squares fitting were obtained for each data set to evaluate possible discrepancies of the model. Due to the large number of spectra, a MATLAB interface was built in order to treat data globally from the raw data.

Ex-situ bipolar electrochemistry treatments of $IrO_x$ for EDX analyses were performed on $IrO_x$ deposited on COP coated with Pt as described above. After $IrO_x$ deposition following the same process described, pieces 10 x 10 mm were cut and immersed in the sodium phosphate buffer, 3 mm in height, without a long term immersion, and various potentials were applied in an electrochemical cell with two parallel 24 mm wide Pt driving electrodes 30 mm apart, in two-electrode configuration. Samples were cleaned with deionized and Millipore water, dried under a $N_2$ stream, and stored in ambient conditions. A clip was used to make good contact between the upper $IrO_x$ layer and the SEM holder before EDX for Na and Ir was measured along the main electric field axis used in the electrochemical set up. Therefore, the results include $K^+$ diffusion or exchange due to concentration gradient in the sample, in addition to $Na^+$ intercalation due to bipolar electrochemistry effects. Measurements are always done scanning in the following order: negative $IrO_x$ side, positive $IrO_x$ pole and geometrical center as expected point of zero charge. If the positive side is measured before, a reduction is detected, evidencing that the electron beam may modify the oxidation state of iridium, and therefore the ionic gradient within the sample, and justifying the use of XRay absorption instead.

Equivalent preparations were made for visual inspection of the bipolar phenomena on the $IrO_x$ coatings. 5 and 7 V were applied between Pt driving electrodes, while a sequence of photographs was taken with lateral light to prevent reflection. The electrolytes used in this case were the same phosphate buffer used for EDX and XAS measurements, and a 0.1 M oxalic acid solution. The resulting gradient material was also studied later by cyclic voltammetry through direct connection, in the same phosphate media.

A finite element simulation was performed using COMSOL Multiphysics software in its electrostatic module was used to estimate the expected dipoles induced in the 2 mm stripes for each potential applied. In addition, a case where both the original $IrO_x$ and the reduced phase were present was considered (Using reported conductivity values of $1.1 \cdot 10^{-2}$ S/cm was used for $IrO_x$ as deposited, and $1.5 \cdot 10^{-6}$ S/cm for the reduced $IrO_x$

[27], presumably Ir (III) state). Geometric cell constrains were equal to the cell described above.

## 3. Results & Discussion

### 3.1. Optical changes

Changes occurring in the Iridium oxidation state are easily visualized through visual inspection given the known electrochromic effect [17]. Figure 2 shows in situ color changes in $IrO_x$ coatings deposited on Pt-COP, in bipolar conditions with various external applied voltages. As observed, the starting $IrO_x$ coating is dark blue in color. Reduction of $IrO_x$ at the induced cathode (-) bleaches that color, and a greyish color remains, partially due to the underlying Pt coating. The spatial front separating the color of positive and negative zones is approximately in the center of the material, considering the direction of the applied electric field, when 7 V (2.3 V/cm) are applied. A closer view shows that in fact there are three regions of color. The extreme corresponding to $IrO_x$ positive pole is darker than the intermediate region, showing different reduction states.

At lower potentials, (5 V, 1.7 V/cm) the color change has not reached the center, but the type of color change is similar at the induced cathode, and a middle intermediate region appears. $O_2$ gas bubbles are also observed at 7 V in the induced $IrO_x$ anode (positive side), in agreement with previous reports [11]. At larger potentials, both $O_2$ and $H_2$ are observed at the positive and negative poles, especially in acid media, while the color indicates that the bipolar change has also occurred.

An estimation of the actual induced dipole in these conditions, based on previous measurements [15] suggests that the external imposed 7 V creates a 0.7 - 1 V between $IrO_x$ borders. On the other hand, the expected dipole, simulated by COMSOL finite element calculations, yields 0.4 V even if a decrease of conductivity of the reduced part occurs (Conductivity data $1.1 \cdot 10^{-2}$ S/cm in the electrodeposited $IrO_x$ to $1.5 \cdot 10^{-6}$ S/cm for the reduced species [27]).

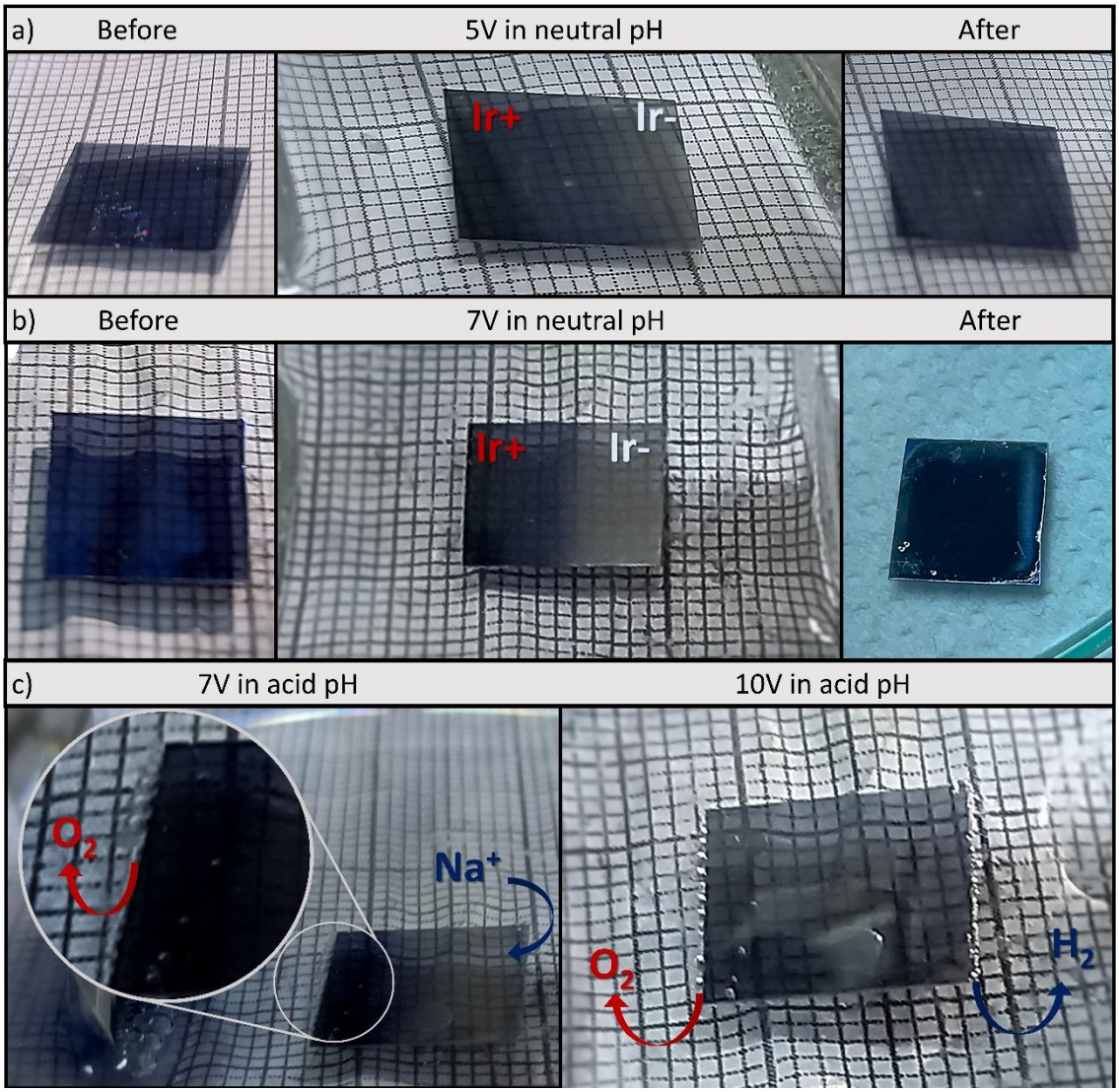


**Figure 2.** Macroscopic images of $IrO_x$ coatings on Pt-COP, prior to a bipolar experiment, during and after, at various potentials. a) 5 V external applied potential at neutral pH, b) 7 V applied potential at neutral pH, c) 7 V and 10 V at acid pH. (Tilted examples at 5 V show how the front is still parallel to the Pt electrodes).

Cyclic voltammetry run, right after the bipolar treatment, through direct contact, evidences what the gradient material is in electrochemical terms. $IrO_x$ sample that has not undergone bipolar treatment shows similar results to those described earlier, with two wide reductions waves at 0.2 and – 0.3 V vs Ag/AgCl. The bipolar piece, with both sides immersed has the same waves, have a similar CV but with the first reduction wave shifted cathodically 0.18 V vs Ag/AgCl. The open circuit potential is lowered by 0.1 V vs Ag/AgCl for the gradient $IrO_x$ treated at 5 V evidencing a larger average reduction, as expected. Both shifts suggest that it is more difficult to reduce the gradient $IrO_x$ since it has a lower oxidation state. On the other hand, the second reduction wave is not reached in such interval of potentials resulting in a more reversible oxidation wave. The width of the peak is also doubled with respect to the original $IrO_x$ CV, evidencing a wider range of potential, as it would be expected from a gradient material.

On the other hand, the CV experiment itself may also be modifying the electron distribution within the pre-existing gradient. Significantly enough, however, direct contact electrodes show reversibility and stable charge capacity above 1000 cycles [18, 21-24], so, these effects are only related to the gradient in $IrO_x$. Moreover, here several cycles coincide with the previous one.

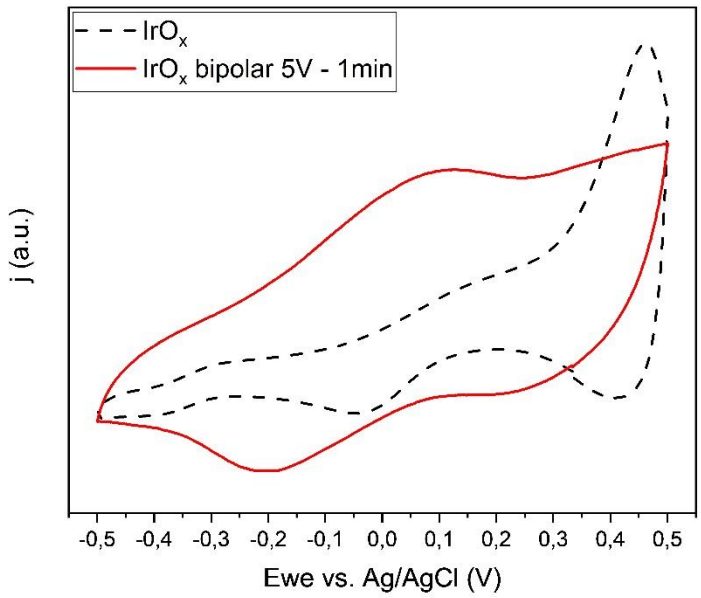


**Figure 3**. Cyclic voltammetry (second cycle), of the precursor $IrO_x$ coating (black) on Pt-COP, and of a $IrO_x$ on Pt-COP treated in bipolar conditions at 5 V, 1 min (red). (Both parts corresponding to Ir+ and Ir- poles immersed for the gradient $IrO_x$).

### 3.2. Ex situ Na EDX in bipolar $IrO_x$

Since previous ECQM studies on $IrO_x$ directly connected as cathode had shown $Na^+$ intercalation [18], it is feasible to study the oxidation state gradient for iridium based on the intercalated $Na^+$ ionic gradient. A 100% efficiency on reduction of Ir resulting in intercalation of $Na^+$ would involve that the amount of $Na^+$ corresponds exactly to the decrease in Ir oxidation state.

EDX $Na^+$ content study is represented in Table 1, along with SEM images of the $IrO_x$ coatings. As the resulting values are considered semiquantitative, the more representative value of Na/Ir atomic ratios at induced cathode, induced anode and center of the sample are shown. The table is shown for various external potentials applied, and several times after the experiment.

At large voltages (7 V), an immediate asymmetry is observed in Na content, being highest at the induced $IrO_x$ cathode. At this voltage, the degree of intercalation observed is around 10% in atomic Na/Ir ratios at the induced cathode, for 1 min bipolar treatments. Such ratio involves a decrease of 0.1 in iridium oxidation state, since $Na^+$ intercalation counterbalances the reduction. Considering the lower voltage experiments

performed here, redox intercalation is expected at the induced $IrO_x$ cathode, also. However, for very small times of sample immersion before the bipolar experiment, $K^+$ is still present in the sample and very large concentration gradients in $K^+$ and $Na^+$ from the sample and electrolyte concentrations may induce a large driving force for diffusion of both ions, beyond any applied electric field. EDX performed short times after the bipolar experiments in sodium phosphate electrolyte show large $Na^+$ contents along the sample, implying that the ionic gradient effect, with a high concentration of Na on the electrolyte, dominates the diffusion of ions.

Longer times after the low voltage experiments show however an evolution on the $Na^+$ concentration within the $IrO_x$ phase, that end with the expected gradient of $Na^+$ within the coating; $Na^+$ larger amount in what had been the $IrO_x$ induced cathode, and no $Na^+$ in what was the induced anode. (See Table 1) Thus, the EDX –SEM experiments show that an initial K/Na diffusion prevails, and after time, even without the electrolyte, the $Na^+$ rearranges as if a persistent dipole still exists, a rather relevant finding. Also remarkable is that a final gradient material in the time scale of weeks, at least in terms of $Na^+$.

As mentioned, at 7 V, the driving force of the dipole creates an immediate clear asymmetry in Na content, showing that the concentration gradient effect has been surpassed by the dipole. This finding is significant because of the parallelism found below in in situ XAS Iridium LIII experiments, in that case with much lower noise. In those cases, immersion prior to the experiment assures that $K^+$ has migrated from the phase.

The 8 V case (2.7 V/cm), with no $Na^+$ intercalated in the material shows the limit in EDX experiments for which $H_2$ and $O_2$ formation reactions prevail. Note that even for the same field applied, we expect such limit to be different in XAS experiments.

**Table 1. SEM images showing the microstructure of $IrO_x$ coatings unchanged after the bipolar treatment, and Na/Ir atomic ratios found in ex-situ EDX of $IrO_x$ coatings after bipolar treatment. (Atomic contents measured along the electric field axis)**

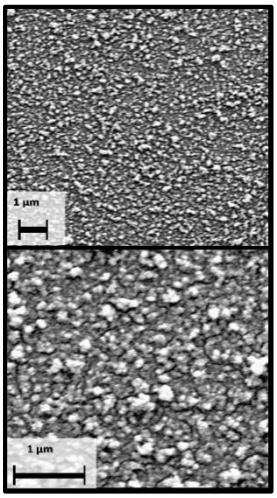


| Electric field | | Measure | Na /Ir atomic ratios on +, center and - sides | | |
|---|---|---|---|---|---|
| **Input voltage** | **V/cm** | | Ir+ | Center | Ir– |
| **5.0V** | **1.67** | after 1hour | 0.09 | 0.09 | 0.08 |
| | | after 1week | 0.00 | 0.10 | 0.07 |
| **6.0V** | **2.00** | after 1hour | 0.15 | 0.11 | 0.10 |
| | | after 1week | 0.00 | 0.05 | 0.04 |
| **7.0V** | **2.34** | after 1hour | 0.00 | 0.11 | 0.07 |
| **7.7V** | **2.57** | after 1hour | 0.00 | 0.05 | 0.07 |
| **8.0V** | **2.67** | after 1hour | 0.00 | 0.00 | 0.00 |

### 3.3. In operando XAS Ir LIII spatial gradient

XAS performed with the vertical cells described in Figure 1 through scanning in the electric field direction evidence Iridium LIII signals shifts less than 1 eV with respect to the $IrO_2$ reference.

All spectra recorded show peaks with nearly the same shape, and no added components are observed during the experiments, and only the maximum energy shifted. The range of imposed external potentials with Pt electrodes 2.6 cm apart, go from 0 to 30 V (where 5, 7 and 8 V correspond to fields 1.9, 2.7 and 3.1 V/cm respectively, in the same range than EDX experiments, 1.7, 2.3 and 2.7 V/cm respectively and larger voltages surpass fields used in EDX experiments).

Examples of spectra of opposing poles in the sample $IrO_x$ stripe, along with a reference of $IrO_2$ ($E_{max}$ 11222.12 eV), are shown in Figure 4. As observed, all $IrO_x$ have negative shift vs $IrO_2$, that is, $IrO_x$ contains Ir with oxidation states below +4. Prior to the use of electric fields, the results found for energy at the maxima ($E_{max}$) agree with previous results reported on anodically deposited $IrO_x$ [18], with $E_{max}$ 11219.09 eV. On the other hand, the difference between absorption energy maxima in positive and negative poles reaches a maximum of 0.7 eV. (As seen below both poles have a lowered $E_{max}$, although larger by max 0.7 eV for the induced cathode)

The fitting described above allows extracting the maxima in energy for each spectra and the full width at medium height for all experiments at various potentials and accumulated processes, with good reliability (least squares factor 0.998 for all cases), and leads to several conclusions described below.

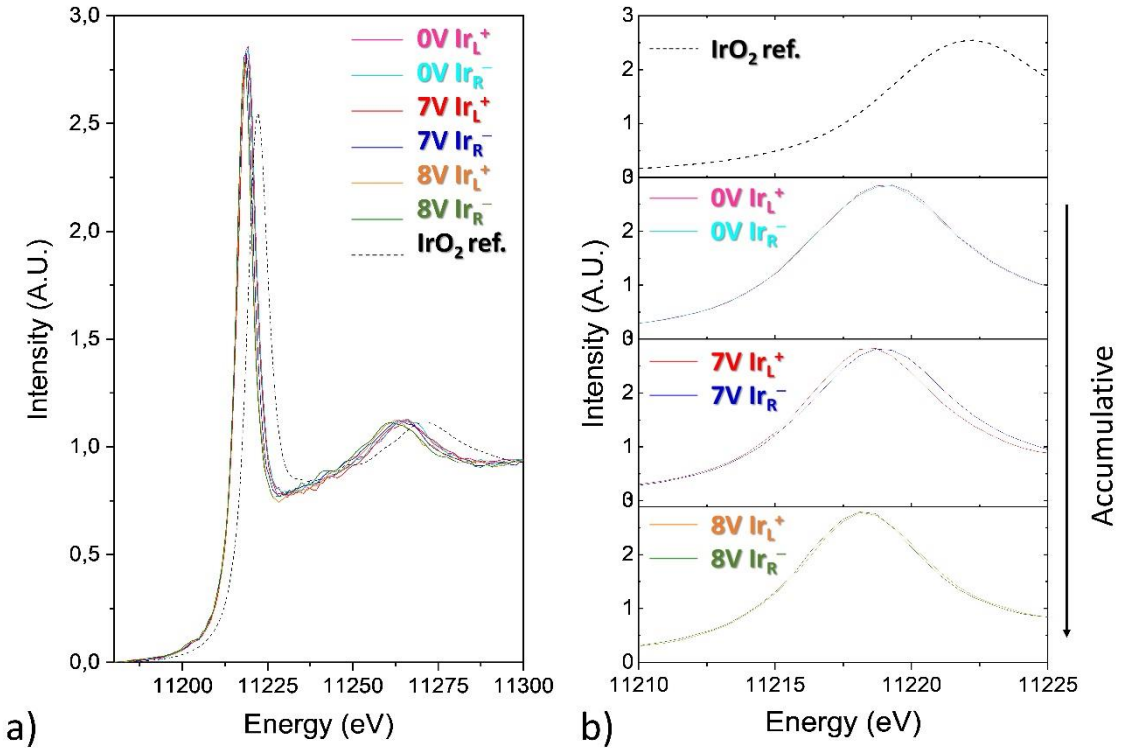

**Figure 4**. a) XAS Iridium LIII after 1 min pulse at 7 V, in opposed stripe positions (Ir induced anode (+) and Ir induced cathode (-), at various consecutive potentials (involving cumulative charge). $IrO_2$ is also shown for reference. b) Main absorption peaks showing the energy shifts for the same cases

Figure 5 shows the variation of the energy at the maximum ($E_{max}$) during a potential ramp from 0 to 5 V between Pt driving electrodes, and after the field is turned off, in a two stripe (A and B) configuration. A continuous decline in energy is observed for the Ir signal at the induced cathode in A (right side of stripe, $Ir_R^-$), as expected, but curiously enough, it is also observed for the induced anode (left side of the stripe, $Ir_L^+$). Both energy values decay with similar changes while the field is acting. However, a bit before the field is turned off, the two signals start to diverge and continue doing so in presence of no field. The difference between both signals remains stable from 400s after the field is turned off (1600s from start of experiment) to about 5000s from start, a total of 3400s. Then, both signals merge and slow reoxidation seems to occur since the $E_{max}$ starts to raise at both points, but even after 11000s, no full reoxidation is reached.

While a decrease in energy is expected for a negative pole where Ir reduction occurs, the only possibility for not seeing an increase in energy at the opposite pole is that Ir is not being oxidized, by the presence of the dipole, but instead other species from the electrolyte are oxidized. The presence of $O_2$ bubbles shown in Figure 2 confirms that oxygen is indeed formed at the induced anode. Therefore, there is a dipole formed by applying 5 V (0.8 V/cm), and two reactions are identified. The number of electrons exchanged at the induced cathode (iridium reduction) and at the induced anode (water oxidation to $O_2$ and possibly oxygen radicals) is theoretically expected to be equal. At the same time, a gradient $IrO_x$ is formed, with Ir absorptions differing 0.3 eV approximately between poles, and the gradient is stable during about 1 hour. For longer times the Iridium LIII peak at both poles reach the same energy and after that reoxidation occurs within the electrolyte in ambient conditions.

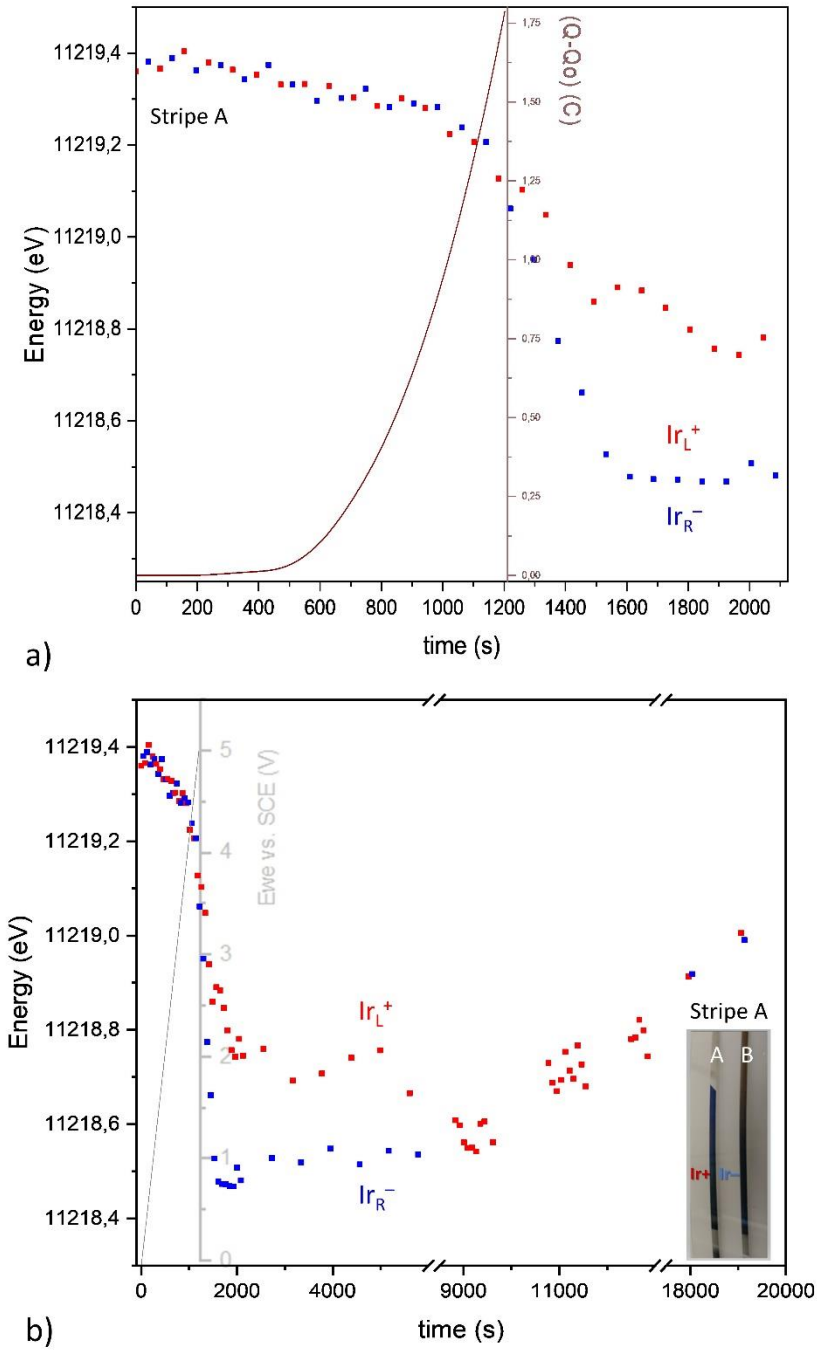


**Figure 5**. A) Energy maxima in Iridium LIII peak observed at extreme negative (blue) and positive (red) poles for $IrO_x$ coating during a ramp 0 to 5 V (1.9 V/cm) and further relaxation (shown by vertical limit). b) Longer relaxation times evidence a quasi-stable difference in energy between positive and negative poles up to 5000s, while longer times show oxidation of the entire sample by atmospheric $O_2$. (NOTE that points in the 3 graphs correspond to the evolution of the measurement with time in the same position (as opposed to graphs below where spatial scans are shown, the first spatial scan in fact). Charge delivery, Q, (not related to bipolar conditions) through driving electrodes and Voltage profile are shown in a) and b) respectively to clarify electric field conditions.

Significantly, stripe B, which is closer to the Pt driving electrode acting as anode, (and where $O_2$ is formed), has a similar behavior, except that the reoxidation that occurs faster. Such $O_2$ however has not affected the bipolar experiment since its effect would have been opposed, and the induced cathode $IrO_x$ would have oxidized, as shown in Figure 1a and d. (Figure S1)

The FWMH values have an almost linear correlation with energy $E_{max}$, as shown in Figure 6, for both the induced anode and the induced cathode. The lower the energy, corresponding to $IrO_x$ reduction, the lower is also the FWMH. Since the cathode reaches a larger reduction, FWMH for the cathode also reaches lower values. In mixed valence phases, like $IrO_x$, with low energy activations for electron transfer, the decrease of the width seems related to the disappearance of mixed valence. That would imply that the cathode reaches the Ir (III) state. The process is not abrupt, and no stabilization is found at the end of the bipolar experiment suggesting that it has not reached the final single state of Ir (III). On the other hand, the existence of the anode would indeed prevent it.

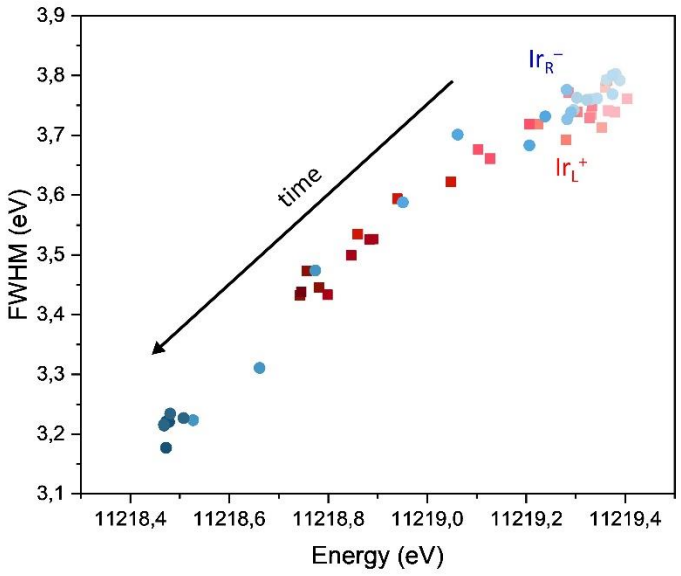


**Figure 6.** Full width at medium height values with respect to Absorption energy for negative (blue) and positive (red) $IrO_x$ poles in stripe A in two stripe experiment. Colors become more intense as the effect grows. Note that both poles decrease its width as well as energy, but the negative pole decreases more.

Although the asymmetric reactions at the $IrO_x$ induced anode and cathode could imply a lack of reversibility, an inversion of the process, a sweep from 0 to -5 V on the same sample was tested after relaxation was allowed. It would seem possible deintercalation of $Na^+$ at the previous induced cathode, becoming now an anode, and intercalation in what used to be the induced anode, now cathode in the inverted field.

The energy changes observed are shown in Figure S2. During the potential scan, no changes are observed. The energy remains in the values observed after relaxation.

However, once the field is stopped, a divergence between previously positive and negative poles (now negative and positive respectively) appears. The pole that used to be negative in the first sweep remains at lower energy, during the relaxation. That implies a clear irreversibility, despite the ambient reoxidation observed, and suggests that $Na^+$ remains intercalated. In such case, reoxidation most probably involves $OH^-$, and $H^+$.

The sudden change after shutting down the electric field in the sweep 0 to 5 V suggested the possible formation of a capacitor, since a charge separation continues, and indeed a slow relaxation. Therefore, the exploration of pulsing the field and allowing for relaxation may follow better the sample equilibrium dynamics. That can be done in two possible ways, exploring different voltage pulses for the same time in each pulse, or using the same voltage (where some process is already known to occur) at different times.

In first place, a pulsed sequence is run in the same potential range, up to 5 V. The results, which are cumulative, are shown in Figure 7. This time, not only the stripe edges are measured but also a whole scan from positive $IrO_x$ to negative $IrO_x$ pole is done. The figure shows the time and space dimensions to clarify that point.

In that potential range, a small difference is seen among poles, although the negative pole is in general lower in energy than the positive pole. In addition, all scans accumulate a reduction effect, which does not correspond to possible interactions from hydrogen, since it affects all the stripe positions. It would rather seem that the reduction at the negative pole propagates towards the positive pole, as in previous experiments. The magnitude of the energy difference corresponding to each scan goes from 0.03 to 0.06 eV, and has a lot of noise in this voltage range. It seems, therefore, that we may still be far from the voltage at which the process occurs. Figure 7b shows the changes in energy during relaxation at one of the voltages used, 3.5 V. As seen, the positive pole is above in energy (as in previous experiment), but in smaller extent, and after 500s the poles reach the same energy, but continue being reduced, and stay reduced at least until 3000s.

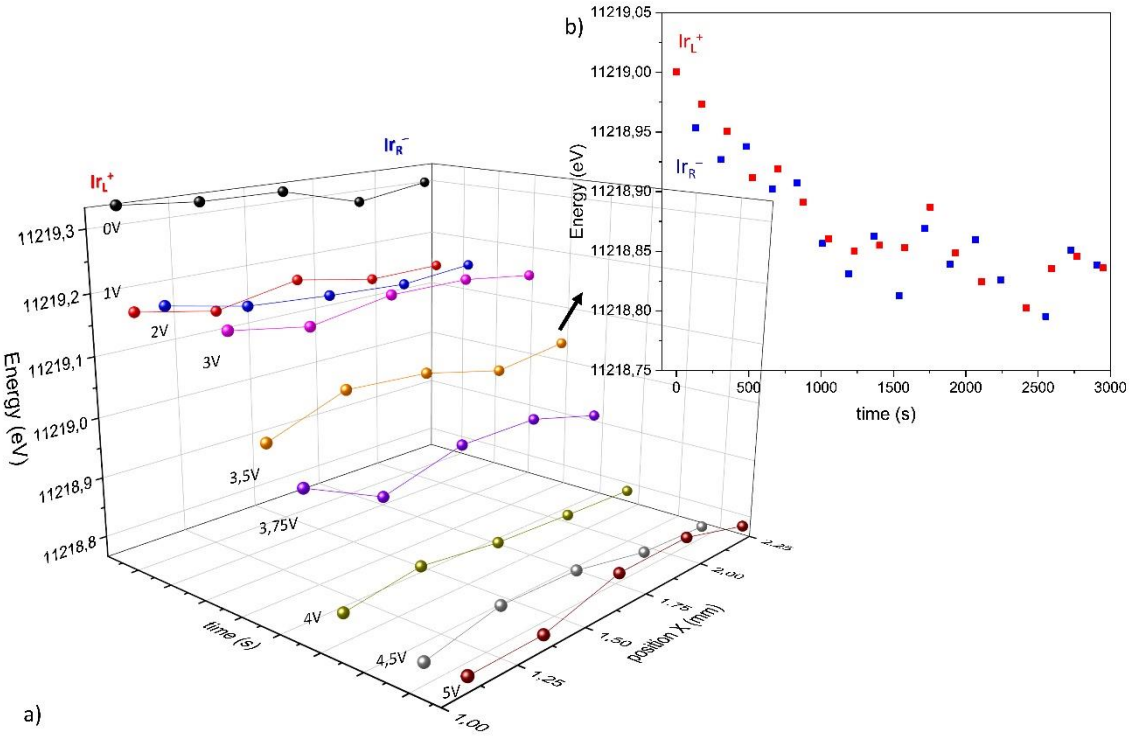


**Figure 7**. a) $E_{max}$ for Iridium LIII peak in several scans performed after 1 min pulses in one-stripe cases at the indicated volts and 1 hour relaxation before next potential. b) Representative 1 hour relaxation after a pulse of 3.5 V 1 min in the one stripe case.

After 10 days of relaxation, the maximum energy of the sample is practically recovered (11219.3 eV), reaching up to 11219.1 eV. A further exploration of larger potentials is therefore done in the pulsing scheme, up to 30 V, to pin the optimal potential in which the process is above noise level. As in a voltammetry, the effects are sequential and cumulative. Because relaxation effects are known, these experiments do not include long relaxations.

Figure 8 shows the energy changes during the larger voltages pulsing sequence, in a one stripe case. The graph is splitted in two parts and b to make it more clear (although they are sequential). Figure 8a, shows that the big jump in energy between poles occurs at 7 V. At 8 V, the accumulative effect shows that the region between 7 and 8 V corresponds to the induced dipole where a largest energy difference in Iridium LIII is found. Two-dimensional projections in E vs time and E vs spatial scan axes show it even more clearly. The maximum energy difference observed between induced poles is 0.03 eV for 5 V, 0.35 eV total for 7 V applied and 0.66 eV total for 8 V. (See sequential pulses and relaxation in Figure 7 and 8). Up to 10 V, the negative $IrO_x$ pole has lower energy than the positive pole (at the left in the scan), but the difference between poles does not increase beyond those values, suggesting that we have reached the maximum reduction possible at the induced $IrO_x$ cathode. Although no reference is possible for Ir (III) oxidation state, it is plausible that this is the end of the attainable reduction, corresponding to an $E_{max}$ for Ir L(III) absorption at 11218.45 eV. Roughly, such reduction in iridium oxidation state would correspond to the maximum $Na^+$ intercalation found in

EDX at the induced cathode, established around 0.1 Na/Ir. Although such value is 1 eV below the one found for starting $IrO_x$ energy $E_{max}$, the difference between poles never reach 1 eV because reduction propagates towards the anode.

Such maximum reduction would correspond to the CV reduction waves observed for directly connected $IrO_x$ electrodes, only in this bipolar experiment it would occur at the induced cathode, and would propagate towards the opposite pole. It would indeed correspond to the maximum $Na^+$ intercalation found in ex-situ EDX experiment. Beyond such voltage, no additional reaction occurs at $IrO_x$.

However, at 12 V, the sign of the Ir oxidation state gradient starts to invert its values. While the left, $IrO_x$ positive side, is still present in the left side of the scan, the last spatial point in the negative $IrO_x$ pole (right side) raises its energy again. At higher potentials, the tendency within each anode towards cathode scan has completely changed its slope with respect to the 7 or 8 V and below. Since such negative pole is in front of the Pt driving anode, producing $O_2$, at these potentials in much larger amount, it is logical to assume that in this range, those $H_2$ and $O_2$ large amounts from Pt may dominate the effect in $IrO_x$. Significantly, it also says that $H_2/O_2$ effect does not influence for potentials below 8 V. Between 8 and 12 V a mixed regime exists, where both, the dipole effects and gas influence appear.

Scheme found in Figure 1d, shows those possible reactions. It is remarkable that the sequence of XAS experiments has pinned the energy changes in $IrO_x$ with gradient oxidation states, the dipole that originates that and the potential range where the reactions derived from the existence of the dipole dominate (case 1), while evidencing the range where gas formation from water splitting at Pt electrodes dominates (case 2). Thus, XAS shows what neural cell studies also established those limits for that specific cell configuration in bipolar regime [11].

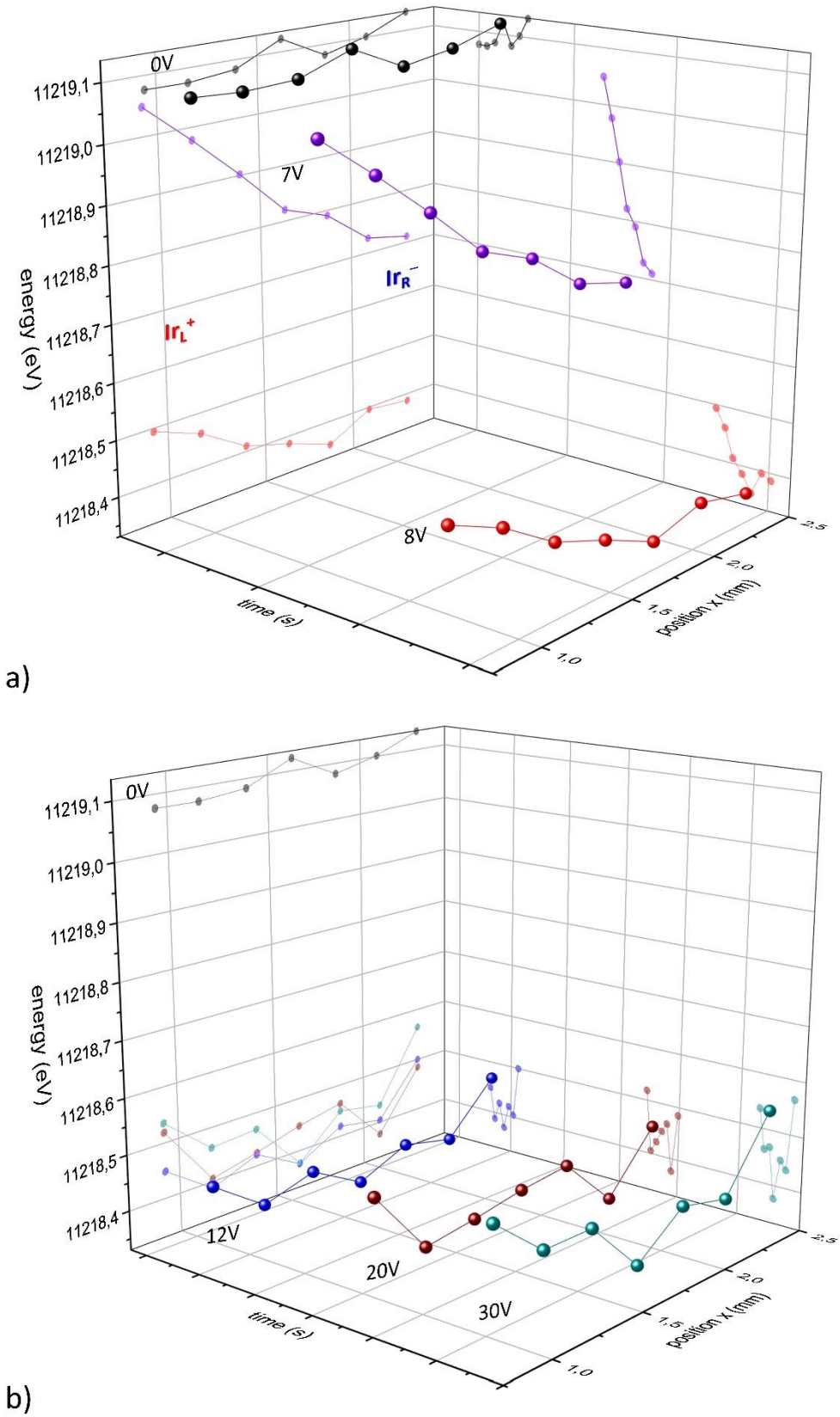


**Figure 8**. Energy for the absorption maxima in Iridium LIII peak in one stripe case, at the indicated voltages. Note that each color is a spatial scan (the first scan) across a stripe for each voltage pulse measured after the pulse. a) 0 V, 7 V and 8 V b) 0 V, 12 V, 20 V and 30 V.

A last experimental pulsed sequence tries to determine the effect of slow kinetics, at potentials near but no superior to the one where the biggest change is observed. Thus, a 5 V sequence is chosen, using a fresh sample (three stripes), where pulsing different times, may determine if the same effect can be obtained by a longer time exposure. The results are shown in Figure 9. In this case, a scan is run thorough the three stripes, to evaluate possible differences, due also to the water splitting at the driving electrodes, or to interaction between them, due to $O_2$ formation at the induced anodes in $IrO_x$

Although strip C has always lower energy than stripe A and B, it cannot be due to $H_2$ produced at the driving Pt cathode, because C is closer to the Pt driving anode that produces $O_2$. Instead, a possible inhomogeneity of $IrO_x$ electrodeposition could be held responsible of the difference, probably due to worst Pt contact along the stripe. The use of several stripes at once therefore helps to establish possible divergences in initial oxidation states.

At this voltage, all scans show noise as before at the same voltage (see Figure 5). Nevertheless, there is also a tendency in some cases. The right negative pole tends to be lower in energy than the center points of the scan (see 12 to 30 V in Figure 8). It would seem as if the dipole middle zero charge point is shifted. In addition, in stripe A and B, the induced cathode has in front the induced anode from the next stripe and $O_2$ produced there. Therefore, this experiment shows the complexity of the interactions between stripes. It is possible that charge transfer occurs between a reduced species at the induced cathode that transfers charge to the immediately close induced anode in the nearby stripe. Therefore, the alternating sequence of induced anodes and cathode offer redox processes if bipolar pieces close enough. Such charge transfer has been observed before when several solid pieces are immersed and a redox soluble species serves as indicator [paper pieces], and explains changes in impedance and charge transfer mechanisms [6], even in suspensions of conducting particles. Therefore, the three stripe case in this work includes additional factors that induce such noise also at the 5 V ramp case (two stripe). Previous 2 and 1 stripe experiments are therefore more clear.

Furthermore, for each stripe as a whole, all points of the horizontal (anode to cathode) scan raise in energy when $O_2$ from the Pt, much larger in amount, predominates. In this case, with three stripes, the right stripe, C, is near the anode, and is the first stripe to show the effect. (In this case at 5 V, for one and two stripes, at 12 V). Discrete measurements through alternative slits also show the effect.

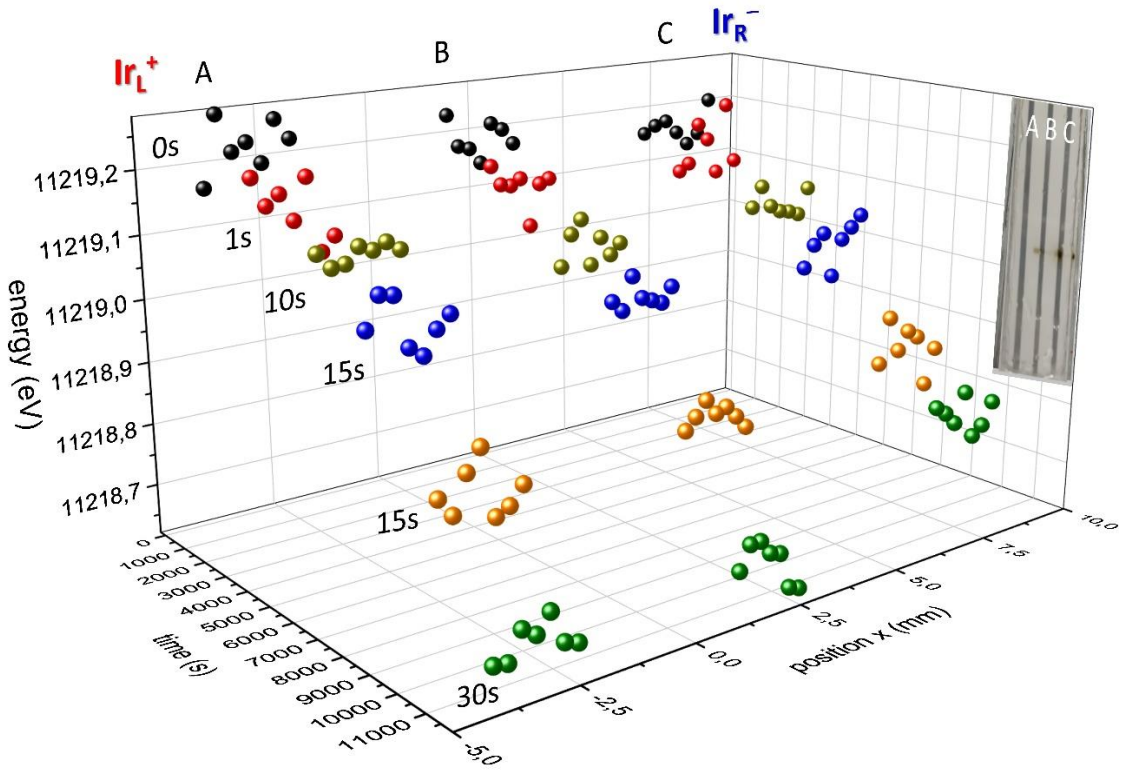


**Figure 9**. Energy vs time by scanning the three stripe for a constant voltage (5 V). Each group corresponds to a scan in strips A (left), B (medium) and C (right) and run from Ir+ pole to Ir- pole each. Note that on the right side (in front of Ir- pole in stripe C is a Pt+ driving electrode generating $O_2$. And that on the left side, in front an Ir+ pole in stripe A, is a Pt- driving electrode. The 3 stripe experiment has two stripes closer to Pt electrodes.

As a summary, from 0 to 8 V applied (field 0 to 4.2 V/cm) in general, the Iridium LIII peak maximum shifts to lower energy in the induced $IrO_x$ cathode as expected from the reduction of iridium. However, in less extent, the energy for Iridium LIII also decreases at the induced $IrO_x$ anode side. Thus, despite the initial Ir oxidation state below IV, no oxidation of Ir occurs at that positive pole, and that involves the existence of an alternative reaction taking place, the electrolyte oxidation ($H_2O$ to $O_2$ or to oxygen radicals, $O^{-n}$). As $IrO_x$ is a known catalyst for $O_2$ evolution, it is highly probable, and Ir may be at the highest possible oxidation state in aqueous media because of such catalytic process. Previous experiments [3] evidence easy delamination of Pt on Ti glass at the induced anodes at certain potentials, while pH indicators show the formation of $H^+$, suggesting the fact that the electrolyte is the one undergoing the oxidation ($H_2O$ to $O_2$), and may also be observed in the gas bubbles at the induced anode in Figure 2.

In addition, the significant decrease in conductivity for the reduced $IrO_x$, may be shifting the point of zero charge, towards the induced anode, inducing a larger portion of reduced $IrO_x$ along the experiment, and explaining the $Na^+$ migration in that direction. Thus, we observing a complex bipolar electrochemistry process that combines the material reduction and water oxidation, plus an evolution of the center zero charge front. Such complexity may be intrinsic for $IrO_x$, mainly because of its catalytic activity in

$O_2$ evolution, and not for other electroactive bipolar electrodes tested in neural cell culture [11], and could explain the different effects on cell growth among materials.

It is worth to remark that, despite geometrical factors, the voltages at which the dipole reaches the maximum value is similar in optical, EDX and XAS experiments (slightly smaller for XAS since Pt driving electrodes are closer). That is so, even although the stripe is narrower than the square piece in EDX, and agrees with reported empirical data for the dipole magnitude as a function of applied voltage [15], and also with COMSOL calculations [33] even although other materials were considered.

When using 1, 2 or 3 stripes the change in energy corresponding to the dipole, is equal among them, and stripes become different in the stripes closer to the driving electrodes and only at the high voltages when $O_2$ and $H_2$ are formed. So, position within the parallel electrode field, does not affect in terms of bipolar electrochemistry effects.

Some additional quantitative data may be extracted from the relaxation observed in gradient $IrO_x$ XAS signals in situ. Relaxation in energy values after field pulses and prior to reoxidation must involve $Na^+$ diffusion, and can be estimated taking into account the cross section through which $Na^+$ ions move and the time required to observe both poles being equal. Without taking into account the influence of change in conductivity, an estimate results of $D = 1.397 \cdot 10^{-12}$ $m^2/s \rightarrow V = 6.986 \cdot 10^{-10}$ m/s similar to other intercalation materials (as compared to $Na^+$ diffusion in water $D = 1.48 \cdot 10^{-5}$ $m^2/s \rightarrow V = 2.96 \cdot 10^{-8}$ m/s). As mentioned, the diffusion mechanism may be driven by concentration gradients, conductivity gradients and redox potentials gradients, all interrelated. In all cases, such diffusion is sufficiently slow to enable the design of *pn*-like devices in such timescale, and additional work is planned in that respect.

The minimum induced dipole, as derived from the energy difference between poles according to XRay absorption is much larger for 7 V than for 4 or 5 V. The maximum energy difference observed is 0.03 eV for 5 V, 0.35 eV total for 7 V applied and 0.66 eV total for 8 V. (See sequential pulses and relaxation in Figure 7 and 8.)

Surprisingly also, for low voltages, the shift in Iridium LIII absorption continues after the electrical field has stopped, evidencing a very slow kinetics of re-equilibration of $Na^+$ ions within the $IrO_x$ amorphous structure, between induced cathode and towards the induced anode, and a possible capacitive effect. The absorption shifts to lower energy for both poles after the field is switched off, with increasing difference among them, the induced cathode increasingly lower, as if the dipole still persists. It is remarkable that this is the same type of behavior observed in SEM-EDX measurements discussed above.

## 4. Conclusions

Spatial gradient in Iridium oxidation states have been observed in situ, for conducting $IrO_x$ in presence of an external driving field, even in the narrow energy range that Iridium LIII line allows. This observation evidences that XAS measurements are a unique method to establish the iridium chemistry changes that neural cells grown in such substrate is sensing. The decrease in energy of absorption of the Iridium L (III) lines in XAS is sufficient to show that Ir is reduced in the induced $IrO_x$ cathode, in agreement with semiquantitative EDX $Na^+$ intercalation results. A smaller reduction of Iridium is also observed at the induced anode, evidencing the propagation of such reduction, while always keeping an energy difference that would correspond to the charge effects of the induced dipole. The electrochemical oxidation process therefore, occurring at the $IrO_x$ induced anode interface, corresponds to $O_2$ formation from $H_2O$. The global reduction state, even in the induced anode side, suggests that neural cells sense an environment less aggressive than the atmospheric oxygen rich electrolytes, and may evidence a reason why $IrO_x$ is one of the best materials as substrates of neural growth and tissue repair. A gradient in such reduced state, along with a related $Na^+$ gradient, also suggests a directionality possible in the substrate that benefits cell growth [18].

The dipole and its effects have a notable persistence in time, as if a capacitor has been created. After several hours, the system relaxes back and the absorption energy gets close to the initial values in atmospheric conditions. Two ranges of potentials are identified, in the first the dipole dominates the gradient observed in Iridium oxidation state through the width of the stripes, but the behavior below 7 V differentiates from the behavior at 3 to 5 V. At 7 V, the process is immediate, while at 3.5 V an accumulation of charge seems to exist (capacitor like effect). In a second zone of potentials, above 10 V, $H_2O$ splitting occurs predominantly, and the gradient at $IrO_x$ is inverted due to the nearby production of $H_2$ and $O_2$ at the driving electrodes.

The dynamics of $Na^+$ migration to equilibrate charge seem to have diffusions similar to other intercalation materials. Significantly, the gradient persists in Na and in Ir oxidation state, in the order of hours, while initial color change from blue to grey disappears into the grey color. Although such color involves an unknown degree of reduction, clearly all parts of the material reach such threshold.

Additional studies in other materials will allow establishing possible differences between the gradients created in various electroactive materials used in bipolar conditions. While $IrO_x$ offers a lower activation energy for oxidation of water, as shown above, which eventually results in a lower gradient than expected, other materials may undergo a different bipolar effect. The effects on neural growth of alternative materials as PEDOT-PSS, where neuron dendrite growth tends towards the induced cathode, could be related to a larger spatial gradient in $M^+$ intercalation, since PEDOT is expected to oxidize also at the induced anode.

**Supplementary Material:** Additional data comparing different stripes and time evolution is available in a Supplementary material file.

**Author Contributions**

The manuscript was written through contributions of all authors. All authors have given approval to the final version of the manuscript. The original idea and the electrochemistry behind have been set by NCP and developed by NCP, LlA and LF. The operando electrochemical cell was designed by NCP, LF, DT and LlA. LlA has participated on sample preparation (Pt deposition, and stripe formation) with LF and NCP, and has designed the raw data treatment. In situ experiments were run by LF, DT, LlA, LS and NCP. LS has contributed through some technical synchrotron details.

**Financing and Acknowledgements**

The authors thanks financing from the Ministry of Science of Spain (MAT2015-65192-R, and RTI2018-097753-B-I00), and Severo Ochoa Program (CEX2019-000917-S). LlA thanks the Ramon y Cajal Program contract (RYC-2013-12640). ALBA synchrotron experiments were performed under Grant 2020024334.

**References**

(1) Shida, N.; Zhou, Y.; Inagi, S. Bipolar Electrochemistry: A Powerful Tool for Electrifying Functional Material Synthesis. Acc. Chem. Res. **2019**, *52*, 2598−2608.
(2) Koefoed, L.; Pedersen, S.U.; Daasbjerg, K. Bipolar electrochemistry—A wireless approach for electrode reactions. Current Opinion in Electrochemistry **2017**, *2,* 13–17.
(3) Tisserant, G.; Fattah, Z.; Ayela, C.; Roche, J.; Plano, B.; Zigah, D.; Goudeau, B.; Kuhn, A.; Bouffier, L. Generation of metal composition gradients by means of bipolar Electrodeposition. Electrochimica Acta **2015**, *179*, 276–281.
(4) Krabbenborg, S.O.; Huskens, J. Electrochemically Generated Gradients, Angew. Chem. Int. Ed. **2014**, *53*, 9152 – 9167.
(5) Braun, T.M.; Schwartz, D.T. Localized Electrodeposition and Patterning Using Bipolar Electrochemistry, J. Electrochem. Soc., **2015**, *162*, D180-D185.
(6) Fattah, Z.; Garrigue, P.; Lapeyre, V.; Kuhn, A.; Bouffier, L. Controlled Orientation of Asymmetric Copper Deposits on Carbon Microobjects by Bipolar Electrochemistry, J. Phys. Chem. C **2012**, *116*, 22021−22027.
(7) Ishiguro, Y.; Inagi, S.; Fuchigami, T. Gradient Doping of Conducting Polymer Films by Means of Bipolar Electrochemistry, Langmuir **2011**, *27*, 7158–7162.
(8) Fosdick, S.E.; Knust, K.N.; Scida, K.; Crooks, R.M. Bipolar Electrochemistry, Angew. Chem. Int. Ed. **2013**, *52*, 10438 – 10456.
(9) Zhou, Y.; Engelberg, D.L. Fast testing of ambient temperature pitting corrosion in type 2205 duplex stainless steel by bipolar electrochemistry experiments. Electrochem. Comm. **2020**, *117*, 106779.

(10) Karimian, N.; Hashemi, P.; Afkhami, A.; Bagheri, H. The principles of bipolar electrochemistry and its electroanalysis applications. Current Opinion in Electrochemistry **2019**, *17*, 30–37.
(11) Rajnicek A.M.; Zhao, Z.; Moral-Vico, J.; Cruz, A.M.; McCaig, C.D.; Casañ-Pastor, N. Controlling Nerve Growth with an Electric Field Induced Indirectly in Transparent Conductive Substrate Materials, Advanced HealthCare Mat., **2018,** *7*, 1800473.
(12) Bhavar, V.; Kattire, P.; Thakare, S.; Patil, S.; Singh, RKP. A Review on Functionally Gradient Materials (FGMs) and Their Applications, IOP Conf. Series: Materials Science and Engineering, **2017**, *229*, 012021.
(13) Munoz-Rojas, D.; Subias, G.; Fraxedas, J.; Gomez-Romero, P.; Casan-Pastor, N. Electronic Structure of Ag2Cu2O4. Evidence of Oxidized Silver and Copper and Internal Charge Delocalization, *J. Phys. Chem. B* **2005**, *109,* 6193-6203.
(14) Munoz-Rojas, D.; Oro, J.; Gomez-Romero, P.; Fraxedas,J.; Casan-Pastor, N. Electrochemically induced reversible solid state transformations: electrosynthesis of Ag2Cu2O4 by room temperature oxidation of Ag2Cu2O3, Electrochem. Commun. **2002,** 4, 684-689.
(15) Chao, H.J.; Lin, Z.S.; Singuru, M.M.R.; Chuang, M.C. Sustainable oxygen-evolving electrode via in situ regenerative deposition of hexahydroxyiridate (IV)-adsorbed IrOx nanoparticles, Electrochimica Acta, **2021,** *383*, 138291.
(16) Tsai, H.M.; Yang, S.J.; Ma, C.C.M.; Xie, X. Preparation and electrochemical activities of iridium-decorated graphene as the electrode for all-vanadium redox flow batteries, Electrochimica Acta, **2012**, *77*, 232– 236.
(17) Gottesfeld, S.; McIntyre, J.D.E.; Beni, G.; Shay, J.L. Electrochromism in anodic iridium oxide, Appl. Phys. Lett, **1978**, *22*, 208-210.
(18) Cruz, A.M.; Abad, Ll.; Carretero, N.M.; Moral-Vico, J.; Fraxedas, J.; Lozano, P.; Subías, G.; Carballo, M.; Collazos-Castro, J.E.; Casañ-Pastor, N. et al, Iridium Oxohydroxide, a Significant Member in the Family of Iridium Oxides. Stoichiometry, Characterization, and Implications in Bioelectrodes, J. Phys. Chem C. **2012**, *116*, 5155–5168.
(19) Cogan, S.F.; Ehrlich, J.; Plante, T.D.; Smirnov A.; Shire, D.B.; Gingerich, M.; Rizzo, J.F.; et al., Sputtered iridium oxide films for neural stimulation electrodes, J Biomed Mater Res B Appl Biomater. **2009**, *89*, 353-61.
(20) Lichtenstein, M.P.; Pérez, E,; Ballesteros, L.; Suñol, C.; Casañ-Pastor, N. Short term electrostimulation enhancing neural repair in vitro using large charge capacity intercalation electrodes. Applied Mat. Today, **2017**, *6*, 29-43.
(21) Perez, E.; Lichtenstein, M.P.; Suñol, C.; Casan-Pastor, N. Coatings of Nanostructured Pristine Graphene-IrOx Hybrids for Neural Electrodes: Layered Stacking and the role of non-oxygenated Graphene, Mat.s Sci. Eng. C, **2015**, *55*, 218-226.
(22) Carretero, N.M.; Lichtenstein, M.P.; Pérez, E.; Cabana, L.; Suñol, C.; Casan-Pastor, N. IrOx-Carbon Nanotubes Hybrid: A Nanostructured Material for Electrodes with Increased Charge Capacity in Neural systems, Acta Biomaterialia, **2014**, *10*, 4548-4558.

(23) Carretero, N.M.; Lichtenstein, M.P.; Pérez, E.; Sandoval, S.; Tobias, G.; Suñol, C.; Casan-Pastor, N. Enhanced Charge Capacity in Iridium Oxide-Graphene Oxide Hybrids. Electrochimica Acta, **2015**, *157*, 369-377.
(24) Pérez, E.; Carretero, N.M.; Sandoval, S.; Fuertes, A.; Tobias, G.; Casañ-Pastor, N. Nitro-graphene oxide in Iridium Oxide hybrids: Electrochemical modulation of N-graphene redox states and Charge capacities, Mat. Chem. Frontiers, **2020**, *4*, 1421 – 1433.
(25) Potrepka, D.M.; Rivas, M.; Ronald, H.Y.; Polcawicha, G.; Aindow, M.; Fox, G.R. Characterization of IrOx sputtering for IrO2 and IrO2/Pt bottom-electrode piezoelectric micro-electro-mechanical systems applications, Thin Solid Films, **2017**, *638*, 127-137.
(26) Mclntyre, J. D. E.; Peck, Jr., W. F.; Nakahara, S. Oxidation State Changes and Structure of Electrochromic Iridium Oxide Films, J. Electrochem. Soc, **1980**, 127, 1264-1268.
(27) Chow, K.F.; Carducci, T.M.; Murray, R.W. Electronic Conductivity of Films of Electroflocculated 2 nm Iridium Oxide Nanoparticles, J. Am. Chem. Soc. **2014**, *136*, 3385−3387.
(28) Rajnicek, A.M.; Suñol, C.; Casañ-Pastor, N. Nanostructured Electroactive Materials with Large Charge Capacity: Direct Field Electrostimulation through Connected and Non-connected Electrodes. in "Engineering Biomaterials for Neural Applications: Targeting Traumatic Brain and Spinal Cord Injuries". Editors: López-Dolado, E.; Serrano, M.C. Chapter 5, Springer Nature **2021**. In press
(29) Hillman, A.R.; Skopek, M.A.; Gurman, S.J. X-Ray spectroscopy of electrochemically deposited iridium oxide films: detection of multiple sites through structural disorder, Phys. Chem. Chem. Phys., **2011**, *13*, 5252–5263.
(30) Reksten, A.H.; Russell, A.E.; Richardson, P.W.; Thompson, S.J.; Mathisen, K.; Seland, F.; Sund, S. An in situ XAS study of high surface-area IrO2 produced by the polymeric precursor synthesis. Phys. Chem. Chem. Phys., **2020**, *22*, 18868.
(31) Nunes, P.S.; Ohlsson, P.D.; Ordeig, O.; Kutter, J.P. Cyclic olefin polymers: emerging materials for lab-on-a-chip applications, Microfluidics and nanofluidics, **2010**, *9*, 145-161.
(32) Simonelli, L.; Marini, C.; Olszewski, W.; Ávila Pérez, M.; Ramanan, N.; Guilera, G.; Cuartero, V.; Klementiev, K. CLAESS: The Hard X-Ray Absorption Beamline of the ALBA CELLS Synchrotron. Cogent Physics **2016**, *3*, 1231987.
(33) Abad, Ll.; Rajnicek, A.; Casañ-Pastor, N. Electric Field Gradients and Bipolar Electrochemistry effects on Neural Growth. A finite element study on immersed electroactive conducting electrode materials. Electrochimica Acta, **2019**, 317, 102-111.

**TOC**